Journal of Contaminant Hydrology 131 (2012) 1–8

Contents lists available at SciVerse ScienceDirect

Journal of Contaminant Hydrology

journal homepage: www.elsevier.com/locate/jconhyd

Diffusive flux and pore anisotropy in sedimentary rocks

C.E. Schaefer [a,*], R.M. Towne [a], V. Lazouskaya [b], M.E. Bishop [c], H. Dong [c]

[a] Shaw Environmental, Inc., 17 Princess Road, Lawrenceville, NJ 08648, United States
[b] Department of Plant and Soil Sciences, University of Delaware, Newark, Delaware, 19716, United States
[c] Department of Geology, Miami University, Oxford, OH 45056, United States

ARTICLE INFO

Article history:
Received 30 August 2011
Received in revised form 9 January 2012
Accepted 10 January 2012
Available online 20 January 2012

Keywords:
Diffusion
Bedrock
Matrix
Anisotropy

ABSTRACT

Diffusion of dissolved contaminants into or from bedrock matrices can have a substantial impact on both the extent and longevity of dissolved contaminant plumes. For layered rocks, bedding orientation can have a significant impact on diffusion. A series of laboratory experiments was performed on minimally disturbed bedrock cores to measure the diffusive flux both parallel and normal to mineral bedding of four different anisotropic sedimentary rocks. Measured effective diffusion coefficients ranged from 4.9×10^{-8} to 6.5×10^{-7} cm^2/s. Effective diffusion coefficients differed by as great as 10-folds when comparing diffusion normal versus parallel to bedding. Differences in the effective diffusion coefficients corresponded to differences in the "apparent" porosity in the orientation of diffusion (determined by determining the fraction of pore cross-sectional area measured using scanning electron microscopy), with the difference in apparent porosity between normal and parallel bedding orientations differing by greater than 2-folds for two of the rocks studied. Existing empirical models failed to provide accurate predictions of the effective diffusion coefficient in either bedding orientation for all four rock types studied, indicating that substantial uncertainty exists when attempting to predict diffusive flux through sedimentary rocks containing mineral bedding. A modified model based on the apparent porosity of the rocks provided a reasonable prediction of the experimental diffusion data.

1. Introduction

The presence of dissolved contaminants in fractured bedrock aquifers poses a challenging environmental problem at many commercial and federal facilities. One complexity in understanding contaminant migration within these systems is the diffusion of contaminants into or out of the rock matrices. Several studies have shown that such diffusion can have a substantial impact on contaminant transport and persistence, affecting the dissolved concentrations in adjacent hydraulically conductive fractures (Goldstein et al., 2004; Holtta et al., 1996; Lange and Van Geel, 2011; Lipson et al., 2005). However, predicting diffusional flux through bedrock matrices is challenging due to difficulties associated with predicting the effective diffusion coefficient through the rock matrix, which has resulted in continued efforts to improve predictions regarding both long and short-term impacts on the dissolved contaminant plume.

For homogeneous isotropic rocks, Boving and Grathwohl (2001) showed that the effective diffusion coefficient through the rock matrix could be described by the following:

$$D_{eff} = D_{aq}\varepsilon^{m} \quad (1)$$

where D_{eff} is the effective diffusion coefficient [cm^2/s], D_{aq} is the solute aqueous diffusivity [cm^2/s], and ε is the physical porosity of the rock matrix. The exponent m was determined to be 2.2 via regression using several rock types.

While Eq. (1) provides a reasonable prediction of the effective diffusion coefficient through homogeneous isotropic rock, the applicability of this correlation for anisotropic rocks has not been fully assessed. Samper et al. (2006) and Wersin et al.

* Corresponding author. Tel.: +1 609 895 5372; fax: +1 609 895 1858.
E-mail address: charles.schaefer@shawgrp.com (C.E. Schaefer).

0169-7722/$ – see front matter © 2012 Elsevier B.V. All rights reserved.
doi:10.1016/j.jconhyd.2012.01.005

(2004) showed that the effective diffusion coefficient was several times greater when diffusion occurred parallel to bedding compared to diffusion normal to bedding for anisotropic claystones. In evaluating siltstone and shale samples, Cavé et al. (2010) showed that the effective diffusion coefficient was 2 to 3-times greater parallel to bedding than normal to bedding. Comparison of the solute-effective porosity to the effective diffusion coefficient in each orientation did not reveal any correlation. Applying Eq. (1) to their data, Cavé et al. (2010) showed that an exponent (m) of 2 to 2.5 was appropriate for diffusion parallel to bedding, while an exponent of 2.5 to 3 was appropriate for diffusion perpendicular to bedding.

Nakashima et al. (2008) employed a combination of X-ray computed tomography (CT) and diffusion simulations to evaluate porosity and diffusion in anisotropic rocks. Results showed that pore anisotropy controlled diffusion. Furthermore, diffusion could be greater in either the parallel or normal orientation.

The objective of this study was to measure and compare the effective diffusion coefficient and apparent porosity (or, pore cross-sectional area) both normal and parallel to bedding in several sedimentary rocks. Diffusive tracer experiments and imaging analysis were performed on each rock type in both orientations in order to obtain experimental measurements of both the effective diffusion coefficient and the apparent porosity in each orientation. Results were compared to the previously developed matrix diffusion model (Eq. (1)). This model was subsequently modified to describe diffusion in anisotropic rock matrices.

2. Materials and methods

2.1. Rock collection and synthetic groundwater preparation

Minimally disturbed rock cores were collected from the former Naval Air Warfare Center (NAWC) in Trenton, New Jersey. Dipping layers of fractured mudstone, siltstone, shale and sandstone of the Lockatong and Stockton Formations are beneath the unconsolidated sediments (Lewis-Brown et al., 2005). The units strike N. 60° E. to N. 70° E. and dip 15° to 20° NW. Each bedding unit consists of several water-bearing zones, alternating with confining zones. Water is transmitted primarily through fractures and joints in the rocks.

Core collection was performed by first drilling a 10 1/4-inch nominal borehole that was advanced through overburden and weathered bedrock using 6 1/4-inch inner diameter (ID) hollow stem augers (HSAs). The HSAs were left in place as temporary casing. A 5 3/4-inch rotary bit and recirculation of drilling fluids (potable water) was used to remove soil and weathered bedrock remaining within the augers. The rotary bit was then advanced until competent bedrock was observed. Rock cores were collected using a triple tube wireline PQ Core Barrel system. This system created a nominal 4.8-inch diameter core hole, and allowed for the collection of minimally-disturbed 3.3-inch diameter rock core sections up to 5 ft in length. Cores were collected using a moderate drilling speed, with moderate, steady down-pressure and sufficient circulation to cool the drilling bit. Three different rock types with visually apparent mineral bedding were collected: a red sandstone (Stockton Formation), a tan sandstone (Stockton Formation), and a dark gray mudstone (Lockatong Formation). In addition, a sandstone block (Arizona Buff) obtained from a commercial quarry, which also contained clearly visible mineral bedding, was used for the diffusion experiments.

A synthetic groundwater (SGW) was prepared based on the groundwater geochemistry at the former NAWC facility. This groundwater was used in all of the diffusion experiments, and consisted of deionized water amended with the following reagent grade chemicals from Sigma-Aldrich (St. Louis, MO): 120 mg/L $CaCl_2$–$2H_20$, 70 mg/L $NaHCO_3$, 0.1 mg/L $NaNO_3$, 60 mg/L $MgSO_4$–$7H_20$, and 4 mg/L KCO. NaOH was added to adjust the pH to 7.7.

2.2. Rock characterization

Sub-samples of rock core were collected to ensure that the coring process did not introduce any artificial microfractures within the rock matrices. Scanning electron microscopy (SEM) was employed to examine small sections of rock core. SEM images taken along the edges (where micro-fracturing due to the coring is most likely to have occurred) were compared to those in the center of the core. A total of 4 core sections were imaged and evaluated.

The collected core sub-samples were too large to place into the SEM sample holder directly. Therefore, a positive replica technique was used with Reprosil® vinyl polysiloxane impression material. Reprosil® vinyl polysiloxane is a degassed material with hydrophilic surface characteristics and excellent dimensional accuracy and detail (<10 μm). Reprosil® is a 1:1 mixture of base to catalyst, which sets in ~10 min. The Reprosil® was spread onto the surface of the core evenly and allowed to set. The mold was then removed from the core surface. Once the mold was created, well-mixed Spurr's resin was poured into the mold to create a positive replica, and the resin was allowed to harden overnight at 70 °C, gold-coated, and viewed in SEM.

The SEM imaging was performed with a Zeiss Supra 35 VP SEM with EDAX Genesis 2000 X-ray energy dispersive spectroscopy (SEM/EDS). The operating voltage was 2 kV. A short working distance (6–10 mm) and low beam current (30–40 mA) were used to achieve the best image resolution.

The total water accessible porosity of each of the four rock types used for the oriented diffusion experiments was determined by measuring the water uptake within the rock. Small slices of rock core (50 to 150 cm^3) were oven dried at 105 °C. The rock disks were subsequently placed in a water bath, with the very top of the rock face above the waterline to allow for escape of air during imbibition. The water uptake experiment continued until moisture equilibrium was established. The effective porosity was estimated by the mass of water taken up by the rock. Total porosity also was estimated by the use of mercury porosimetry. The technique involves the intrusion of mercury at high pressure into a rock through the use of a porosimeter. The pore size can be determined based on the external pressure needed to force the mercury into a pore against the opposing force of the mercury's surface tension.

Several researchers also have employed the use of SEM with image analysis to provide an estimate of the porosity based on 2-dimensional imaging (Bruckschen et al., 2005;

Pye, 1984; Ruzyla, 1986; Ziel et al., 2008). These techniques use the fraction of porous area measured in 2-dimensions to estimate the 3-dimensional porosity (Ziel et al., 2008). Thus, SEM-measured porosity is actually a measure of the effective pore cross-sectional area in the orientation (e.g., normal or parallel to bedding) of the image. It has been well established that the pore cross-sectional area (or formation factor) can be a function of orientation in rocks (Dullien, 1992; Worthington, 2001). Here, we employ the use of SEM to estimate an "apparent porosity" both normal and parallel to bedding. Although porosity is a scalar quantity that is independent of orientation, our use of "apparent porosity" incorporates the effects of pore cross-sectional area associated with bedding orientation. In a similar approach, Desbois et al. (2010) noted differences in "porosity fabric" in clay cross sections normal and parallel to bedding, where a clear difference in the pore cross-sectional area was observed in the presented SEM images. Sato and Suzuki (2003) hypothesize that differences in this pore cross-sectional area (or, apparent porosity) as a function of orientation could be responsible for the anisotropic diffusion observed in their experiments. For our analysis, SEM images collected from thin sections cut normal and parallel to bedding were analyzed with the Image J software (NIH) to determine apparent porosity (based on the pore cross-sectional area) in each orientation. The whole range of brightness of the images was divided into multiple intervals, and the lowest level was considered for porosity. This brightness setting was periodically checked against standards of known porosity. The resulting porosity was also manually checked against water uptake measurements.

Mineralogy of each rock type also was assessed. Ferrous and total iron contents were determined using the 1,10-phenanthroline method (Amonette and Templeton, 1998) and direct current plasma emission spectrometry, respectively. X-ray diffraction (XRD) was employed to further assess rock mineralogy. Quantitative mineralogical analysis was performed using the RockJock program (Eberl, 2003; Srodon et al., 2001) (Table 1) which calculates the proportion of a mineral in a complex mixture by comparing the integrated intensity of a characteristic diffraction peak of that mineral to the intensity of the same peak of an internal standard.

2.3. Rock preparation and diffusion cell construction

A diffusion cell was constructed to hold thinly-cut slices of rock core, oriented either parallel or normal to bedding, so that tracer diffusion across the rock slice could be measured. The conceptual design of the diffusion cell is based on the design of Boving and Grathwohl (2001). The body of the designed cell (Fig. 1) consists of two stainless steel custom-made flanges (Morrill Industries, Inc., Escalon, CA). The volume of each half was approximately 0.5 L, where one half served as the source reservoir and the other half as the sink reservoir for the diffusion experiment. The top of each flange contained two sampling ports. The sampling ports consisted of Swagelock® fittings (Penn Fluid System Technologies, Huntingdon Valley, PA) and valves (Supelco, Milwaukee, WI). PTFE sealant (GORE™ Joint Sealant, W. L. Gore & Associates, Elkton, MD) was used to ensure that no leaks occurred at the sampling ports.

Rock sections were cut from the rock cores using a diamond blade electric saw. Rock sections were typically 5 to 10 cm long and 0.5 to 2 cm thick. Rocks were cut so that sections were obtained in orientations both parallel and normal to bedding for each rock type. An additional water uptake test was performed to verify that the surface of the rock was not altered by the cutting procedures. Water uptake into two similarly sized rocks was measured, where one rock had a saw-cut face, and the other rock face had been naturally fractured. The rate of water uptake into the rocks was nearly identical, indicating that the procedure of saw-cutting the rock did not substantially alter the surface permeability of the rock, and would not impact our measurement of effective diffusivity through the rock.

After cutting the rock, each section was mounted on a thin base of aluminum sheeting (0.2 cm diameter) using J B Kwik epoxy adhesive (J-B Weld, Sulphur Springs, TX). A rectangular opening was cut in the aluminum so that the face of the rock section was not covered by the aluminum. The aluminum base was cut so that it would fit between the flanges of the diffusion cell. The edges of the rock also were sealed with epoxy so that diffusion could occur only normal to the rock surface (which can be either normal or parallel to bedding), from the source reservoir to the sink reservoir.

Table 1
Characterization of rock mineralogy and porosity.

Rock type	Mineralogy (%)	Ferrous iron (mmol/g)	Total iron (mmol/g)	SEM apparent porosity	Water accessible porosity	Hg intrusion porosity
Red sandstone	Albite (51.5), quartz (36), montmorillonite (6.4), muscovite (2.5), hematite(2.2), goethite (0.9), siderite (0.2), biotite (0.1), lepidocrocite (0.1)	0.01	0.03	Normal: 0.074 ± 0.004 Parallel: 0.069 ± 0.007	0.061	0.057
Tan sandstone	Quartz (48), albite (39), tourmaline (0.5), pyrophyllite (10), muscovite (2.5)	0.005	0.09	Normal: 0.068 ± 0.005 Parallel: 0.085 ± 0.002	0.079	0.071
Dark gray mudstone	Dolomite (28), calcite (9), pyrite (5), anorthite (3), microcline (2), orthoclase (2), quartz (2)	0.30	0.96	Normal: 0.050 ± 0.006 Parallel: 0.11 ± 0.005	0.089	0.080
Quarry sandstone	Quartz (100)	0.003	0.02	Normal: 0.085 ± 0.013 Parallel: 0.037 ± 0.012	0.069	0.075

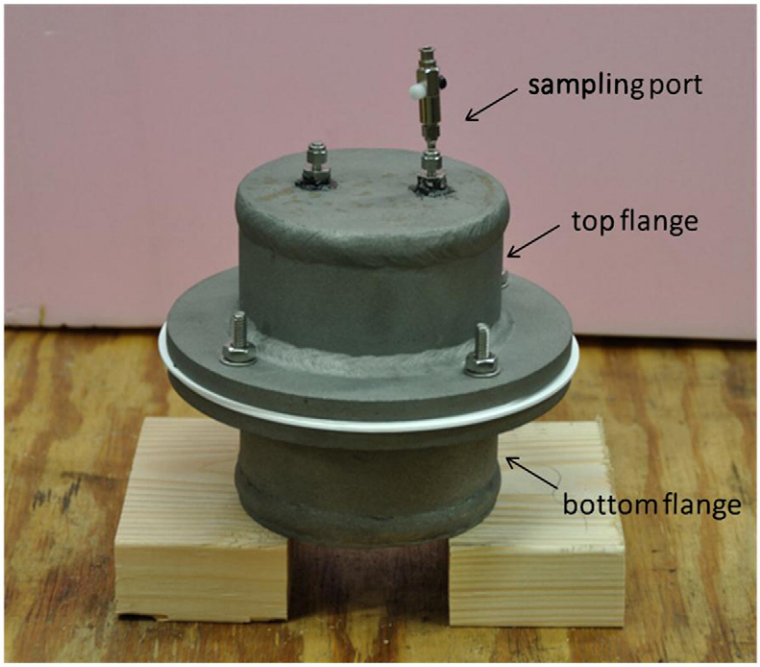

Fig. 1. Diffusion cell used to measure the effective diffusion coefficient through the cut rock sections.

Before inserting the aluminum sheet and rock between the flanges of the diffusion cell, the rock was saturated with SGW. The Viton® gaskets were used to obtain a seal between the flanges and aluminum sheet. Bolts (1/4 in.) were used to fasten and secure the flanges and aluminum sheet-mounted rock.

2.4. Diffusion experiments

Once the diffusion cell was assembled with the mounted wetted rock sample, both the source and sink reservoirs were filled with the initial SGW solutions. The source reservoir was amended with KI for a final concentration of 0.0158 M KI, and the sink reservoir contained iso-osmotic solution of 0.0158 M KNO_3. Experiments were performed at room temperature (approximately 20 °C).

Aqueous samples (1 mL volume) from the sink reservoir were periodically collected. Initial and final aqueous samples also were collected from the source reservoir. Collected samples were analyzed for iodide via ion chromatography (Dionex DX-120, Sunnyvale, CA). Experiments were performed at least in duplicate for each rock type and orientation. For all experiments, the aqueous volume removed during sampling was less than 5% of the total water volume, and the tracer concentration on the sink side of the chamber remained below 2% of the source side tracer concentration.

2.5. Calculation of effective diffusion coefficients

Under steady state conditions, it has been shown (Boving and Grathwohl, 2001; Crank, 1995) that the mass of iodide per cross-sectional area that has migrated to the sink side of the diffusion cell across a rock of thickness d can be described by the following linear equation:

$$M = \frac{C_0 D_{eff}}{d} t - \frac{C_0(\varepsilon + K_d \rho)d}{6} \quad (2)$$

where M is the mass of solute per cross-sectional area that has migrated to the sink side of the diffusion cell [mg/cm^2], C_0 is the initial iodide concentration in the source reservoir [mg/cm^3], d is the rock thickness [cm], t is the time [s], K_d is the iodide sorption coefficient to the rock [cm^3/mg], and ρ is the rock density [mg/cm^3]. Plotting M versus t, and for the case where the iodide concentration on the sink side of the cell is much less than the iodide concentration on the source side of the rock, calculation of the steady-state slope from the experimental data can be used to determine the effective diffusion coefficient of iodide through the rock. Linear regressions were used to determine D_{eff} for each rock diffusion experiment.

3. Results and discussion

3.1. Rock mineralogy and porosity

Initial SEM images of cored material all indicated that there was no significant micro-fracturing that occurred during the drilling process. Images taken from the edges of the cores were similar to those in the center of the core with nearly identical porosity distribution. No artificial fractures were visible near the edges of the cores. These results suggest that no alteration of the rock porosity occurred during the coring process, and no artificial microfracturing occurred.

Rock porosity and mineralogy are summarized for each rock type in Table 1. SEM images for each rock type, which were used to determine the apparent porosity in the parallel and normal to bedding orientations, are provided in Fig. 2. Based on the water uptake and mercury intrusion testing, the effective porosity for each rock is similar, ranging between 6% and 9%. However, a broader range of apparent porosities (3.7% to 10.7%) was observed using the SEM imaging. This broader range was due to the fact that for two of the rock types (the quarry sandstone and the dark gray mudstone), the apparent porosity differed by approximately a factor of two between the parallel and normal orientations. For the quarry sandstone, the SEM-calculated apparent porosity was greater in normal to bedding compared to parallel to bedding; for the dark gray mudstone, the SEM-calculated apparent porosity was greater in parallel to bedding compared to normal to bedding. The porosities for the tan sandstone and red sandstone were similar in each orientation. It is significant to note that, in all cases, the average apparent porosity (normal and parallel to bedding) for each rock was approximately equal to the porosity measured via water uptake and mercury intrusion, thereby confirming that the apparent porosity measured via SEM (and based on the fraction of pore cross-sectional area in each orientation) provided a reasonable description of the porosity. Similar agreement between fractional pore cross-sectional area and porosity was observed by Yokoyama and Nakashima (2005).

Mineralogical analyses of the rocks show that the rocks vary in their mineral composition (Table 1). All rocks contain measurable levels of total and ferrous iron. Total and ferrous

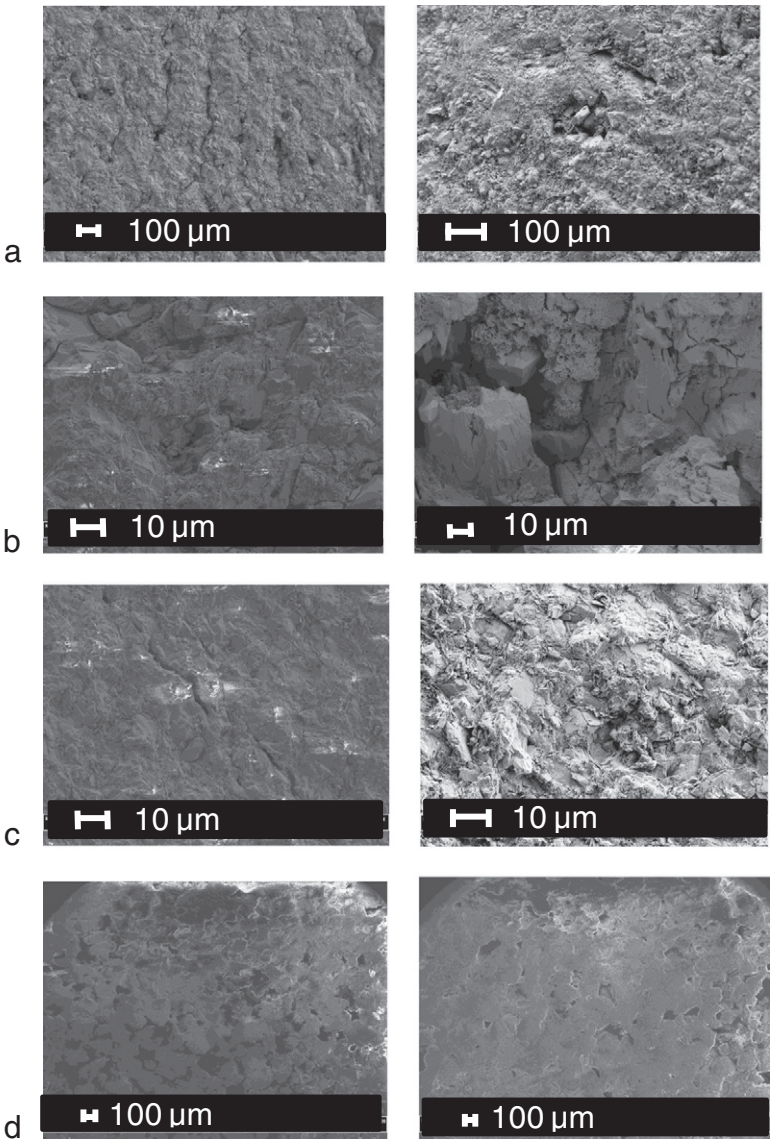

Fig. 2. SEM images of normal (left) and parallel (right) orientations for the a) red sandstone, b) tan sandstone, c) dark gray mudstone, and d) quarry sandstone. Multiple SEM images were collected for each sandstone orientation.

iron levels range from 0.02 mmol/g and 0.003 mmol/g (respectively) in the quarry sandstone, to 1.2 mmol/g and 0.38 mmol/g (respectively) in the dark gray mudstone.

3.2. Effective diffusion coefficients

A typical iodide diffusion curve, based on measured iodide concentrations in the sink reservoir of the diffusion cell, is shown in Fig. 3. The initial non-linear unsteady-state portion of the diffusive elution curve, which occurred within the first 12 days for the experiment shown in Fig. 3, was not used in the linear regression. The regressed slope was used in Eq. (2) to determine the effective diffusion coefficient. The standard errors of the effective diffusion coefficients calculated from regression of the slope for individual diffusion experiments were less than 13% of the regressed value (and were typically less than 8% of the regressed value). Effective diffusion coefficients measured in each rock for both diffusion parallel and normal to mineral bedding are shown in Table 2. Results indicate that the regressed diffusion coefficients were reasonably repeatable. Tests performed on separately cut rock sections for the dark gray mudstone and red sandstone suggest that the rock sections used within the diffusion cell were generally representative of the local rock geology (with respect to iodide diffusion). The magnitude of the measured effective diffusion coefficients are within the range measured by others for sedimentary rocks (Boving and Grathwohl, 2001; Cavé et al., 2010; Descostes et al., 2008).

For the red sandstone, no significant difference in the magnitude of the effective diffusion coefficient was observed when comparing diffusion parallel and normal to bedding. For the tan sandstone, a slightly greater effective diffusion coefficient was observed parallel to bedding compared to normal to bedding. For the dark gray mudstone, diffusion parallel to bedding was approximately 7-times greater than diffusion normal to bedding; diffusion was approximately 10-times greater perpendicular to bedding than parallel to bedding in the quarry sandstone.

These results, consistent with the observations of others (Cavé et al., 2010; Esteban et al., 2006; Van Loon et al., 2004), show that bedding orientation can have a substantial impact on the effective diffusion coefficient through the rock. What is further demonstrated in this current work is that the effective diffusion coefficient anisotropy is directly related to the apparent porosity anisotropy (or fraction of pore cross-sectional area) as determined via SEM imaging. The extent of available pore cross-sectional area controls the rate of diffusion. For the red sandstone, where no statistical difference in SEM-measured apparent porosity is observed as a function of bedding orientation, no anisotropy is observed for the effective diffusion coefficient. For the tan sandstone, where the SEM-measured apparent porosity is slightly greater in the parallel to bedding compared to normal to bedding, the effective diffusion coefficient correspondingly is slightly greater in the parallel orientation compared to the perpendicular orientation. Similar correspondence is demonstrated in the quarry sandstone and dark gray mudstone, where a substantially greater SEM-measured apparent porosity in one orientation corresponds to an increased effective diffusion coefficient in that same orientation. Thus, the apparent porosity as measured by SEM provides an explanation for the differences in the effective diffusion coefficient in parallel versus normal bedding orientations, as the change in apparent porosity (or fraction of pore cross-sectional area) relative to a given bedding orientation results in a proportional change in the effective diffusion coefficient. These experimental coupled apparent porosity and diffusion measurements are in qualitative agreement with the diffusion simulations performed by Nakashima et al. (2008).

Table 2
Measured effective diffusion coefficients for each rock type and orientation. ± values represent the standard error.

Rock type	Number of experiments	Effective diffusion coefficient (cm^2/s)
Red sandstone	Normal: 2	Normal: $1.8 \pm 0.6 \times 10^{-7}$
	Parallel: 4[a]	Parallel: $2.3 \pm 0.4 \times 10^{-7}$
Tan sandstone	Normal: 2	Normal: $1.3 \pm 0.4 \times 10^{-7}$
	Parallel: 3	Parallel: $1.9 \pm 0.4 \times 10^{-7}$
Dark gray mudstone	Normal: 3[b]	Normal: $4.9 \pm 1.3 \times 10^{-8}$
	Parallel: 3[b]	Parallel: $2.8 \pm 0.5 \times 10^{-7}$
Quarry sandstone	Normal: 3	Normal: $6.5 \pm 1.1 \times 10^{-7}$
	Parallel: 2	Parallel: $6.8 \pm 0.8 \times 10^{-8}$

[a] Three separate cut rock sections were used.
[b] Two separate cut rock sections were used.

3.3. Model application

Applying the relationship indicated in Eq. (1), the effective diffusion coefficient divided by the iodide aqueous diffusivity (2.0×10^{-5} cm^2/s) (Cussler, 1984) is plotted versus the water accessible porosity measured via water uptake, similar to the approach employed by Boving and Grathwohl (2001) (Fig. 4). Examination of Fig. 4 reveals that the model does not provide a good prediction of the experimental data, with model predictions varying by up to an order of magnitude from the experimental results. There also does not appear to be any correlation between water uptake porosity and the effective diffusion coefficient for the rock samples used in this study. In addition, the modeling approach of Eq. (1) does not describe the substantial differences in the diffusion as a function of orientation that was observed in some of the rock types.

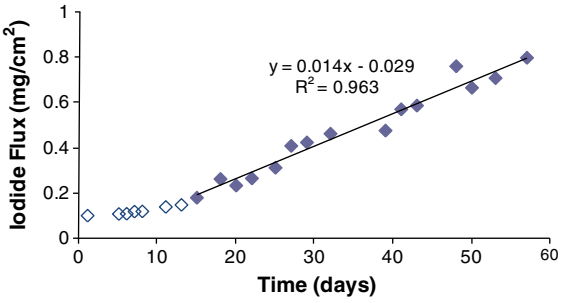

Fig. 3. Iodide diffusion data (quarry sandstone). Non-filled symbols were not used in the regression, as these data were collected during the initial unsteady-state phase of the experiment. The slope, intercept, and correlation coefficient for the regression are shown.

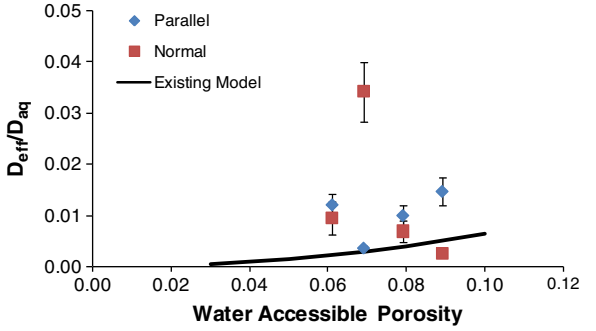

Fig. 4. Prediction of the experimental data using Eq. (1) (existing model based on Boving and Grathwohl (2001)). Error bars represent the standard error.

To describe diffusion through rocks with mineral bedding, the model presented in Eq. (1) is modified as follows:

$$D_{eff} = D_{aq}\varepsilon_o{}^{m} \quad (3)$$

where ε_o is the apparent porosity measured in a specific orientation (i.e., normal or parallel to bedding), as measured via SEM, and m is an empirical fitting parameter. Applying Eq. (3) for each rock type and orientation, and with a best-fit value of m of 1.7, model predictions versus the experimental data are shown in Fig. 5. Results indicate that the modified model presented in Fig. 5 provides a substantially improved prediction of the experimental data, with model predictions falling within a factor of two of the experimental data, which is similar to the level of model accuracy previously observed for Eq. (1) with isotropic rocks (Boving and Grathwohl, 2001). The quarry sandstone (normal orientation) is an apparent outlier, which is not readily explained. The regressed value of m in Eq. (3) is similar to the exponent obtained by others using Eq. (1), where previous values of m for rocks have ranged from 1.6 to 3 (Adler et al., 1992; Boving and Grathwohl, 2001; Cavé et al., 2010; Descostes et al., 2008). The model presented in Eq. (3) also describes the impact of bedding orientation on the effective diffusion coefficient, thereby relating rock physical properties to observed diffusion behavior.

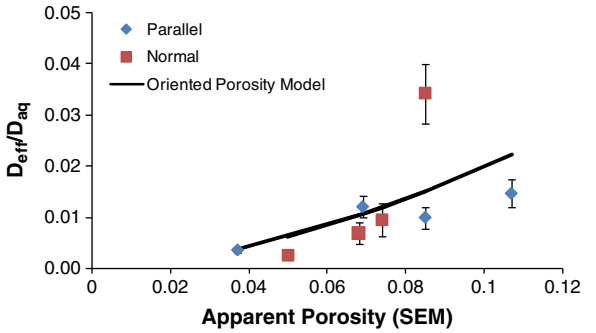

Fig. 5. Prediction of the experimental data using the apparent porosity model (Eq. (3)). Error bars represent the standard error.

4. Conclusions

This study has shown that bedding orientation in sedimentary rocks can have a substantial impact on the magnitude of the effective diffusion coefficient. The magnitude of the diffusion coefficient was related to the apparent porosity (or fraction of pore cross-sectional area) measured via SEM, which depended upon the bedding orientation (either normal or parallel). Using a slightly modified form of an existing model relating rock porosity to the effective diffusion coefficient, a new model was developed based on the SEM-measured apparent porosity. This new model provided a reasonable prediction of the experimental data.

Acknowledgments

The authors thank the Strategic Environmental Research and Development Program (SERDP) for providing financial support for this research. The authors also are appreciative of the guidance provided by Pierre Lacombe of the United States Geological Survey (USGS) for the rock core collection.

References

Adler, P.M., Jacquin, C.G., Thovert, J.F., 1992. The formation factor of reconstructed porous media. Water Resources Research 28, 1571–1576.
Amonette, J.E., Templeton, J.C., 1998. Improvements to the quantitative assay of nonrefractory minerals for Fe(II) and total Fe using 1, 10 Phenanthroline. Clays and Clay Minerals 46, 51–62.
Boving, T.B., Grathwohl, P., 2001. Tracer diffusion coefficients in sedimentary rocks: correlation to porosity and hydraulic conductivity. Journal of Contaminant Hydrology 53, 85–100.
Bruckschen, B., Seitz, H., Buzug, T.M., Tille, C., Leukers, B., Irsen, S., 2005. Comparing different porosity measurement methods for characterization of 3D printed bone replacement scaffolds. Biomedizinische Technik 50, 1609–1610.
Cavé, L., Al, T., Xiang, Y., Loomer, D., 2010. Investigations of diffusive transport processes in sedimentary rock. Nuclear Waste Management Organization, TR-2010-04, Toronto, Ontario, CA. .
Crank, J., 1995. The Mathematics of Diffusion, Second edition. Oxford Science Publications.
Cussler, E.L., 1984. Diffusion — Mass Transfer in Fluid Systems. Cambridge University Press.
Desbois, G., Urai, J.L., De Craen, M., 2010. In-situ and direct characterization of porosity in Boom Clay (Mol site, Belgium) by using novel combination of ion beam cross-sectioning, SEM and cryogenic methods. External Report of the Belgian Nuclear Research Centre10/MDC/P-26, ISSN 1782-2335. .
Descostes, M., Blin, V., Bazer-Bachi, F., Meier, P., Grenut, B., Radwan, J., Schlegel, M.L., Bruschaert, S., Coelho, D., Tevissen, E., 2008. Diffusion of anionic species in Callovo-Oxfordian argillites and Oxfordian limestones (Meuse/Haute-Marne, France). Applied Geochemistry 23, 655–677.
Dullien, F.A.L., 1992. Porous Media — Fluid Transport and Pore Structure. Academic Press, Inc., San Diego, CA.
Eberl, D.D., 2003. User guide to RockJock — a program for determining quantitative mineralogy from X-ray diffraction data: US Geological Survey open file report OF 03-78.
Esteban, L., Géraud, Y., Bouchez, J.L., 2006. Pore network connectivity anisotropy in Jurassic argillite specimens from eastern Paris Basin (France). Physics and Chemistry of the Earth 32, 161–169.
Goldstein, K.J., Vitolins, A.R., Navon, D., Parker, B.L., Chapman, S., Anderson, G.A., 2004. Characterization and pilot scale studies for chemical oxidation remediation of fractured shale. Remediation Journal 14, 19–37.
Holtta, P., Hakanen, M., Hautojarvi, A., Timonen, J., Vaatainen, K., 1996. The effects of matrix diffusion on radionuclide migration in rock column experiments. Journal of Contaminant Hydrology 21, 165–173.
Lange, K., Van Geel, P.J., 2011. Physical and numerical modelling of a dual-porosity fractured rock surrounding an in-pit uranium tailing management facility. Canadian Geotechnical Journal 48, 365–374.
Lewis-Brown, J.C., Carleton, G.B., Imbrigiotta, T.E., 2005. Hydraulic and solute-transport properties and simulated advective transport of contaminated ground water in a fractured-rock aquifer at the Naval Air Warfare Center,

West Trenton, New Jersey, 2003. U.S. Dept. of the Interior, U.S. Geological Survey, Scientific Investigations Report, pp. 2005–5049.
Lipson, D.S., Kueper, B.H., Gefell, M.J., 2005. Matrix diffusion-derived plume attenuation in fractured bedrock. Ground Water 43, 30–39.
Nakashima, Y., Kamiya, S., Nakano, T., 2008. Diffusion ellipsoids of anisotropic porous rocks calculated by X-ray computed tomography-based random walk simulations. Water Resources Research 44 article number W12435.
Pye, K., 1984. Rapid estimation of porosity and mineral abundance in back-scattered electron images using a simple SEM image analyzer. Geological Magazine 121, 81–84.
Ruzyla, K., 1986. Characterization of pore space by quantitative image analysis. SPE Formation Evaluation 1, 389–398.
Samper, J., Yang, C., Naves, A., Yllera, A., Hernández, A., Molinero, J., Soler, J.M., Hernán, P., Mayor, J.C., Astudillo, J., 2006. A fully 3-D anisotropic numerical model of the DI-B in situ diffusion experiment in the Opalinus clay formation. Physics and Chemistry of the Earth 31, 531–540.
Sato, H., Suzuki, S., 2003. Fundamental study on the effect of an orientation of clay particles on diffusion pathway in compacted betonite. Applied Clay Science 23, 51–60.
Srodon, J., Drits, V.A., McCarty, D.K., Hsieh, J.C.C., Eberl, D.D., 2001. Quantitative X-ray analysis of clay bearing rocks from random preparations. Clays and Clay Minerals 49, 514–528.
Van Loon, L.R., Soler, J.M., Muller, W., Bradbury, M.H., 2004. Anisotropic diffusion in layered argillaceous rocks: a case study with Opalinus clay. Environmental Science & Technology 38, 5721–5728.
Wersin, P., Van Loon, L.R., Soler, J.M., Yllera, A., Eikenberg, J., Gimmi, T., Hernan, P., Boisson, J.Y., 2004. Long-term diffusion experiments at Mont. Terri: first results from field and laboratory data. Applied Clay Science 26, 123–135 abstract from ANDRA meeting, Reims, FR.
Worthington, P.F., 2001. The influence of formation anisotropy upon resistivity–porosity relationships. Petrophysics 42, 83–92.
Yokoyama, T., Nakashima, S., 2005. Diffusivity anisotropy in a rhyolite and its relation to pore structure. Engineering Geology 80, 328–335.
Ziel, R., Haus, A., Tulke, A., 2008. Quantification of the pore size distribution (porosity profiles) in microfiltration by SEM, TEM and computer image analysis. Journal of Membrane Science 323, 241–246.